Radiology

Computer-aided Volumetry of Part-Solid Lung Cancers by Using CT: Solid Component Size Predicts Prognosis[1]

Shinichiro Kamiya, MD
Shingo Iwano, MD
Hiroyasu Umakoshi, MD
Rintaro Ito, MD
Hironori Shimamoto, MD
Shota Nakamura, MD
Shinji Naganawa, MD

Purpose: To investigate the relationship between the postoperative prognosis of patients with part-solid non–small cell lung cancer and the solid component size acquired by using three-dimensional (3D) volumetry software on multidetector computed tomographic (CT) images.

Materials and Methods: A retrospective study by using preoperative multidetector CT data with 0.5-mm section thickness, clinical records, and pathologic reports of 96 patients with primary subsolid non–small cell lung cancer (47 men and 49 women; mean age ± standard deviation, 66 years ± 8) were reviewed. Two radiologists measured the two-dimensional (2D) maximal solid size of each nodule on an axial image (hereafter, 2D MSSA), the 3D maximal solid size on multiplanar reconstructed images (hereafter, 3D MSSMPR), and the 3D solid volume of greater than 0 HU (hereafter, 3D SV_{0HU}) within each nodule. The correlations between the postoperative recurrence and the effects of clinical and pathologic characteristics, 2D MSSA, 3D MSSMPR, and 3D SV_{0HU} as prognostic imaging biomarkers were assessed by using a Cox proportional hazards model.

Results: For the prediction of postoperative recurrence, the area under the receiver operating characteristics curve was 0.796 (95% confidence interval: 0.692, 0.900) for 2D MSSA, 0.776 (95% confidence interval: 0.667, 0.886) for 3D MSSMPR, and 0.835 (95% confidence interval: 0.749, 0.922) for 3D SV_{0HU}. The optimal cutoff value for 3D SV_{0HU} for predicting tumor recurrence was 0.54 cm^3, with a sensitivity of 0.933 (95% confidence interval: 0.679, 0.998) and a specificity of 0.716 (95% confidence interval: 0.605, 0.811) for the recurrence. Significant predictive factors for disease-free survival were 3D SV_{0HU} greater than or equal to 0.54 cm^3 (hazard ratio, 6.61; P = .001) and lymphatic and/or vascular invasion derived from histopathologic analysis (hazard ratio, 2.96; P = .040).

Conclusion: The measurement of 3D SV_{0HU} predicted the postoperative prognosis of patients with part-solid lung cancer more accurately than did 2D MSSA and 3D MSSMPR.

[1] From the Department of Radiology (S.K., S.I., H.U., R.I., H.S., Shinji Naganawa) and Department of Thoracic Surgery (Shota Nakamura), Nagoya University Graduate School of Medicine, 65 Tsurumai-cho, Showa-ku, Nagoya 466-8550, Japan. Received September 29, 2017; revision requested December 5; final revision received December 22; accepted January 9, 2018. **Address correspondence to** S.I. (e-mail: *iwano45@med.nagoya-u.ac.jp*).

S.I. supported by Grants-in-Aid for Scientific Research from the Japanese Ministry of Education, Culture, Sports, Science and Technology (KAKENHI; no. 15K09919).

Primary lung cancer is one of the most common malignant tumors in the world. Prognosis of advanced lung cancer has been so poor that early diagnosis is important. Non–small cell lung cancer is classified into solid and subsolid tumors. Subsolid tumors can be further classified into part-solid and nonsolid types based on thin-section computed tomographic (CT) findings. A large number of part-solid tumors are adenocarcinomas, including ground-glass opacity that reflects replacement of the alveolar epithelium by well-differentiated tumor cells, often filled with mucous, and a solid component that reflects intratumoral collapse of airspace or fibrosis (1–4). For the part-solid tumors, several studies have indicated that solid size (the maximal diameter of the solid component) correlates more accurately with tumor invasiveness and prognosis than does total size (the maximal diameter of the whole tumor, including ground-glass opacity [5–9]). The solid size measurement has been adapted as the clinical T factor in the eighth version of the Union for International Cancer Control TNM classification for subsolid lung cancer (2,10).

Conventionally, the maximal total size and maximal solid size have been measured on a two-dimensional (2D) axial CT image (hereafter, 2D MTSA and 2D MSSA, respectively). Multidetector CT enables three-dimensional (3D) whole lung scan and the maximal total size and maximal solid size can be measured on the axial, coronal, and sagittal views by using multiplanar reconstruction of near-isotropic voxels (hereafter, 3D MTSMPR and 3D MSSMPR, respectively). Moreover, volumetry by using computer-aided diagnosis has been able to automatically measure the 3D volume of the whole tumor (total volume [TV]) and solid component (solid volume [SV]) (hereafter, 3D TV and 3D SV, respectively) (11–15). A recent study reported that 3D SV of lung adenocarcinomas can more accurately predict pathologic lymph node metastases and tumor invasiveness than can 2D MSSA (14). This finding indicates that 3D SV enabled prediction of prognosis for subsolid lung cancer. However, determining the border between the ground-glass opacity and solid component in a subsolid tumor is subjective and a cause for confusion on thin-section multidetector CT images.

In our study, we compared 2D MSSA, 3D MSSMPR, and 3D SV with respect to their predictive ability for disease-free survival in subsolid non–small cell lung cancer. We also evaluated the most suitable cutoff value in CT Hounsfield units of the solid component to more accurately predict postoperative recurrence.

Implication for Patient Care

- Computer-aided volumetry of the solid component of a part-solid nodule at CT imaging can accurately predict postoperative recurrence of primary lung cancer.

Materials and Methods

Our retrospective, single-center study was approved by our institutional review board and written informed consent was waived on March 16, 2017 (approval no. 2016–0507).

Patients

Figure 1 shows the flowchart of our study population. By using the retrieval function of the picture archiving and communication system, we searched our institutional database for CT and pathologic reports of patients with pathologically confirmed, surgically resected non–small cell lung cancers between November 2006 and December 2013. During this period, 246 subsolid non–small cell lung cancers were detected in our institution. First, synchronous or metachronous lung cancers (n = 46) and tumors greater than 5 cm in maximal pathologic diameter (n = 4) were excluded from our cohort. The remaining 196 subsolid non–small cell lung cancers were classified into the following three categories: *(a)* postoperative recurrence was observed (n = 15), *(b)* pathologic local invasiveness (pleural invasion, lymphatic invasion, vascular invasion, or lymph node metastasis) was found in the postoperative specimen (n = 31), and *(c)* neither recurrence nor pathologic invasiveness were observed (n = 150). Category 1 (n = 15), category 2 (n = 31), and one-third of category 3 by using a random number table (n = 50) were recruited for further analysis, resulting in a total of 96 patients with subsolid non–small cell lung cancer (47 men and 49 women; mean age ± standard deviation, 66 years ± 8). The mean ages of men and women were 66 years ± 7 (range, 45–78 years) and 66 years ± 8 (range, 42–79 years), respectively. No significant difference was shown in age between men and women (P = .989). The patient demographics and tumor characteristics are shown in Table 1.

The clinical records of all recruited patients were reviewed to obtain data on patient age, sex, date of CT and surgery, surgical procedure, and postoperative course. Lobectomy and pneumonectomy were regarded as standard

https://doi.org/10.1148/radiol.2018172319

Content codes: CH CT

Radiology 2018; 287:1030–1040

Abbreviations:

AUC = area under the receiver operating characteristics curve
MSSA = maximal solid size on axial image
MSSMPR = maximal solid size on multiplanar reconstructed images
MTSA = maximal total size on axial image
MTSMPR = maximal total size on multiplanar reconstructed images
SV = solid volume
SV_{0HU} = solid volume of greater than 0 HU
3D = three-dimensional
TV = total volume
2D = two-dimensional

Author contributions:

Guarantors of integrity of entire study, S.K., S.I., R.I., Shinji Naganawa; study concepts/study design or data acquisition or data analysis/interpretation, all authors; manuscript drafting or manuscript revision for important intellectual content, all authors; approval of final version of submitted manuscript, all authors; agrees to ensure any questions related to the work are appropriately resolved, all authors; literature research, S.K., S.I., Shinji Naganawa; clinical studies, S.K., S.I., H.U., H.S., Shota Nakamura, Shinji Naganawa; statistical analysis, S.K., S.I.; and manuscript editing, all authors

Conflicts of interest are listed at the end of this article.

Figure 1

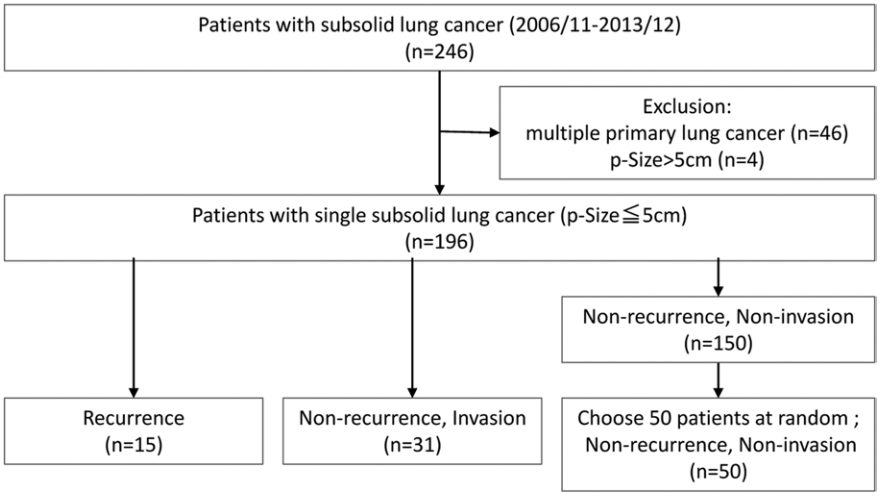

Figure 1: Flowchart of study population.

Table 1

Patient and Tumor Characteristics

Parameter	No. of Patients	Mean ± SD	Median	Range
Female	49	…	…	…
Age (y)	…	66 ± 8	68	42–79
Male	47	…	…	…
Age (y)	…	66 ± 7	67	45–78
Smoking history (pack-year)	…	22 ± 34	0	0–174
Nonsolid/part-solid	4/92	…	…	…
Primary lesion site: RUL/RML/RLL/LUL/LLL	31/2/18/33/12	…	…	…
Limited surgery/standard surgery	18/78	…	…	…
Adenocarcinoma/adenosquamous carcinoma	95/1	…	…	…
Pleural invasion	36	…	…	…
Lymphatic invasion/vascular invasion	6/4	…	…	…
Lymph node metastasis	7	…	…	…
Pathologic tumor size (cm)	…	2.18 ± 0.89	2.0	0.5–5.0
Pathologic stage: 0/I/II/III/IV	1/85/5/5/0	…	…	…
Interval between CT and surgery (d)	…	23.7 ± 24.8	17.5	2–148
Postoperative follow-up duration (mo)	…	60.6 ± 28.8	60	1–120

Note.—RUL = right upper lobe, RML = right middle lobe, RLL = right lower lobe, LUL = left upper lobe, LLL = left lower lobe, SD = standard deviation.

surgery, and wide-wedge resection and segmentectomy were recorded as limited surgery. Pathologic information including tumor size, histologic type, pleural invasion, vascular and lymphatic invasion, nodal metastasis, desmoplastic reaction, and TNM staging were recorded from the final postoperative histopathologic reports. The degree of intratumoral desmoplastic reaction based on the research of Maeshima et al (16) has been recorded routinely in the histopathologic reports at our institution.

The patients were scheduled for follow-up every 1 to 3 months for 2 years after surgery and every 6 months thereafter. Multidetector CT of the chest and abdomen was performed every 6 to 12 months according to the physicians' recommendation. When recurrence was suspected, additional imaging surveys or biopsy were performed.

Three-dimensional CT Scan Protocol

All preoperative 3D CT scans were obtained with a 64-row multidetector CT scanner (Aquilion 64; Toshiba Medical, Tokyo, Japan) in the craniocaudal direction during inspiration without contrast material enhancement by using the following scan parameters: x-ray tube voltage, 120 kVp; automatic tube current modulation, maximum of 500 mA; gantry rotation speed, 0.5 sec; and beam collimation, 64 × 0.5 mm. Axial thin-section multidetector CT images of the whole lung were reconstructed with a section thickness of 0.5 mm at the same increment by using a high-spatial-frequency algorithm (FC52; Toshiba Medical). The iterative reconstruction technique was not used because the multidetector CT scanner at the time could not reconstruct images with iterative reconstruction.

Size and Volume Measurement on a 3D Workstation

All reconstructed thin-section CT images were transferred to a commercially available 3D workstation (VINCENT, version 4.3; Fujifilm Medical, Tokyo, Japan). The axial multiplanar reconstructed and 3D images of extracted nodules were displayed with window level and width settings of 600 HU and 1800 HU and reviewed independently by a radiology resident and a chest radiologists (S.K., with 1 year of experience and S.I., with 22 years of experience reading thoracic CT scans, respectively). The average of the two radiologists' measurements was used for analysis. For the resident, any pretraining for this study was not performed. The two readers knew the measurement objective was subsolid lung cancer, although they did not know the pathologic findings and prognosis. No time limit was set for measurement.

Figure 2 shows the measuring method used to determine the total size and solid size in a subsolid nodule. First, only the maximal total size as 2D MTSA and the

Figure 2

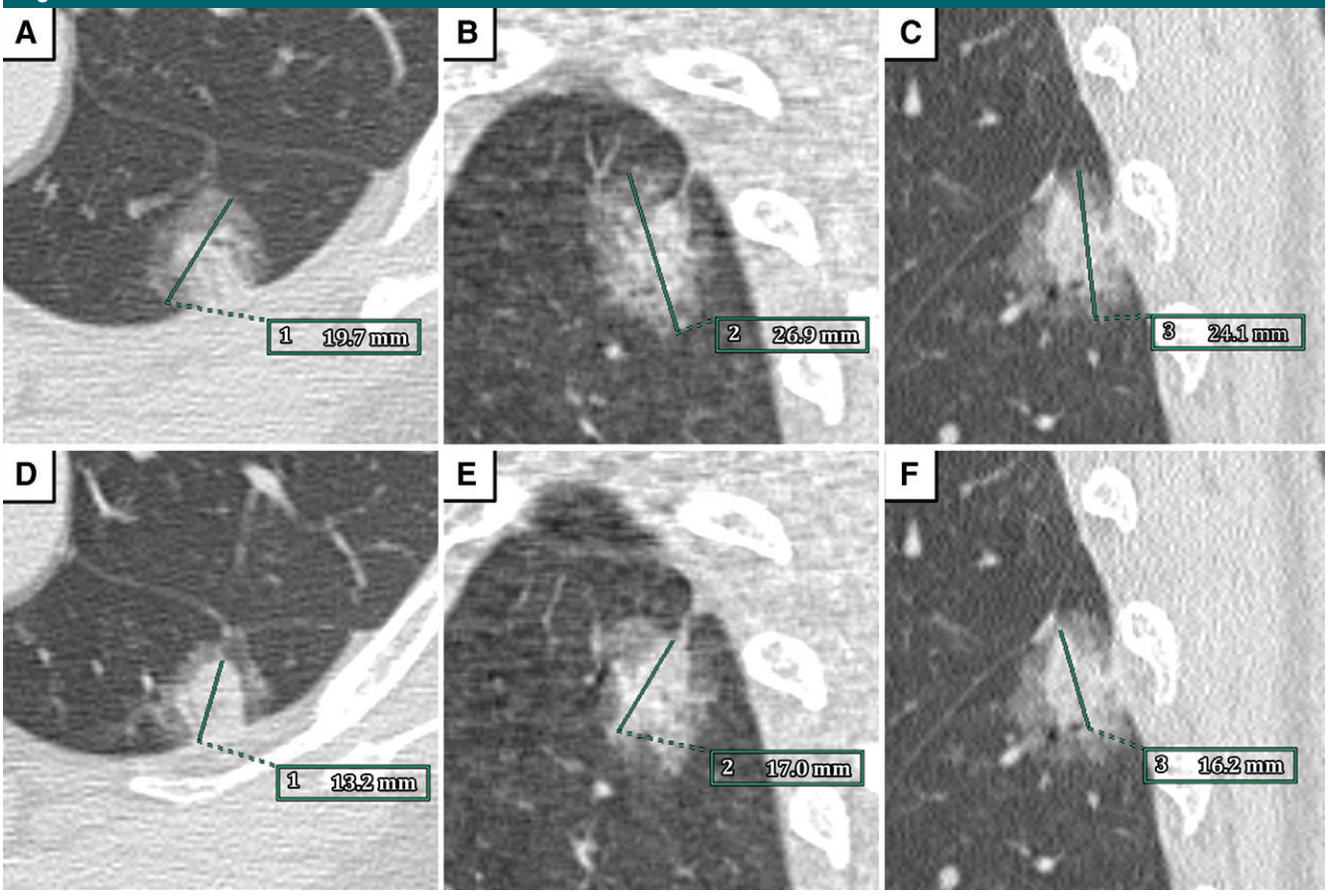

Figure 2: Images show measurements of two-dimensional (2D) maximal solid size on axial image (hereafter, 2D MSSA) and three-dimensional (3D) maximal solid size on multiplanar reconstructed images (hereafter, 3D MSSMPR) on the workstation. *A,* Total size on axial image. *B,* Total size on coronal image. *C,* Total size on sagittal image. *D,* Solid size on axial image. *E,* Solid size on coronal image. *F,* Solid size on sagittal image. For this tumor, 2D maximal total size on axial image and 2D MSSA are 19.7 mm and 13.2 mm, respectively. Three-dimensional maximal total size on multiplanar reconstructed images and 3D MSSMPR are 26.9 mm and 17.0 mm, respectively.

maximal solid size as 2D MSSA on the original axial images were measured. Next, we independently measured the maximal total size as 3D MTSMPR and the maximal solid size as 3D MSSMPR on axial, sagittal, and coronal images with multiplanar reconstruction. Figure 3 shows the measuring method of TV and SV by using computer-aided volumetry. After an observer marked a candidate nodule by dragging the mouse across the nodule, the program automatically defined the margin of interest around the candidate nodule and the margin was displayed on the axial, sagittal, and coronal planes with multiplanar images. If the solid component could not be automatically separated from the chest wall or blood vessels, then the reader manually removed them. When the observer approved the definition of the margin, the program automatically calculated the internal volume for each CT number. We defined a volume based on having a density of greater than −800 HU in the candidate nodule as the 3D TV to eliminate the internal bronchus and any areas of pseudocavitation. In addition, we defined volumes of greater than −300 HU, greater than −200 HU, greater than −100 HU, and greater than 0 HU in the candidate nodule, respectively.

Statistical Analysis

First, the interreader reliability between the two readers (S.K. and S.I.) was analyzed with intraclass correlation coefficient. The degree of agreement was interpreted as follows: less than 0.20, poor agreement; 0.21–0.40, fair agreement; 0.41–0.60, moderate agreement; 0.61–0.80, substantial agreement; and 0.81–1.00, almost perfect agreement (17). Second, patient and tumor characteristics were compared between recurrent and nonrecurrent tumors. Age, duration of postoperative follow-up, tumor size, and tumor volume were compared with Student *t* or Welch *t* test, and distribution of sex, frequency of pathologic invasiveness, and desmoplastic reaction were compared with the χ^2 test. Third, receiver operating characteristic analysis and

Figure 3

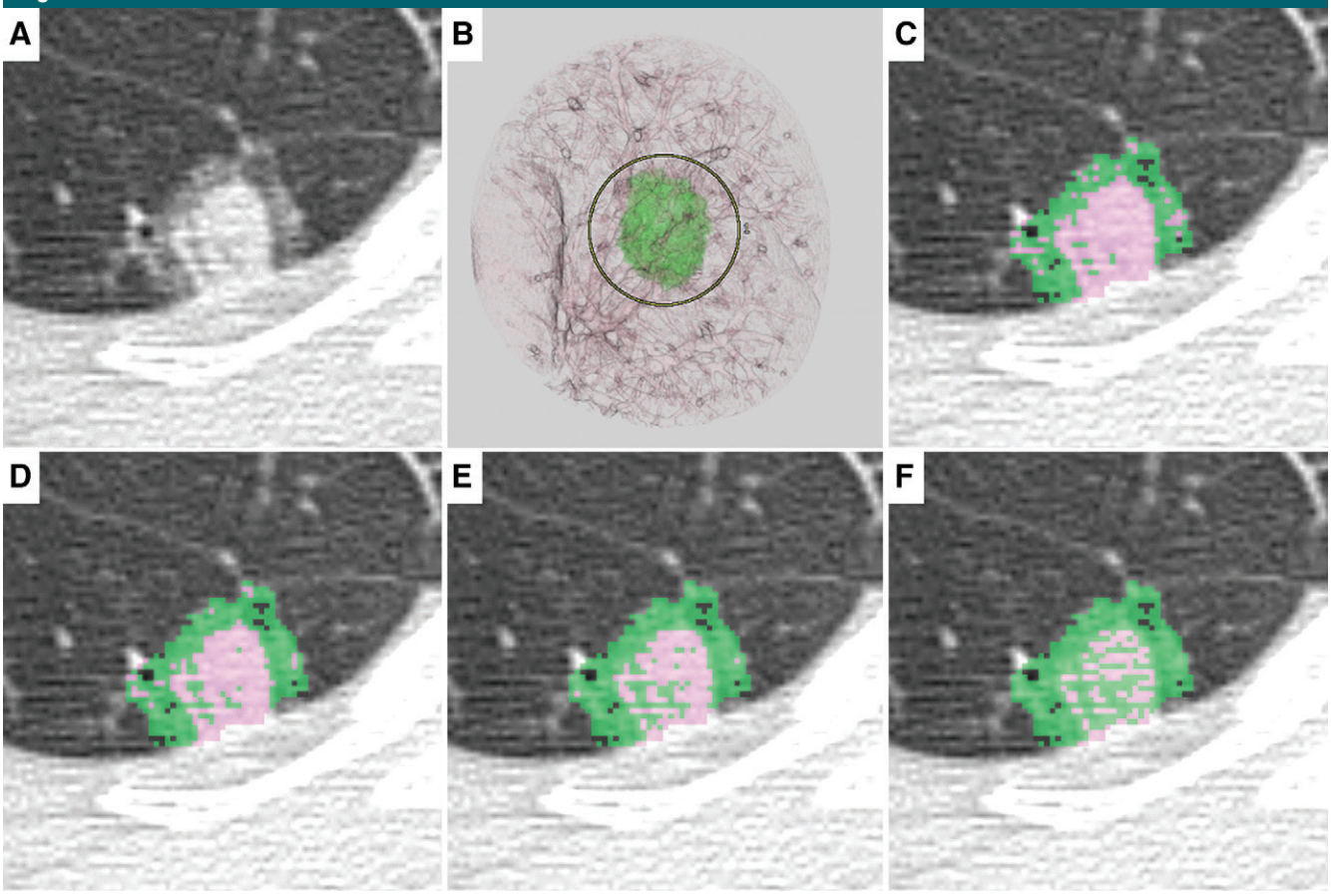

Figure 3: Images show three-dimensional (3D) total volume (hereafter, 3D TV) and 3D solid volume (hereafter, 3D SV) measurements of subsolid nodule by using computer-aided diagnosis. *A,* Axial image of subsolid nodule. *B,* After an observer marks the candidate nodule by dragging the mouse across the nodule, the program automatically defines margin of interest around the candidate nodule and margin is displayed on multiplanar images. When observer approves definition of margin, the program automatically calculates internal volume for each CT number. *C,* Pink area on nodule shows solid part greater than −300 HU and green area shows ground-glass opacity. Volume colored green plus pink is 3D TV. *D,* Pink area on nodule shows solid part greater than −200 HU. *E,* Pink area on nodule shows solid part greater than −100 HU. *F,* Pink area on nodule shows solid part greater than 0 HU.

Youden index were used to determine the suitable cutoff size (in centimeters), CT number (in Hounsfield units), and SV (in cubic centimeters) that would indicate a recurrent tumor. Each area under the receiver operating characteristics curve (AUC) was compared by using the χ^2 test. Fourth, disease-free survival was assessed by using the Kaplan-Meier method, and the survival curves for each subgroup by the cutoff value of 3D SV were compared by using log-rank test. Disease-free survival was defined as the interval between surgery and first disease recurrence, including local-regional recurrence and distant metastasis, or death from any cause. At univariable and multivariable analysis of disease-free survival, Cox proportional hazards model was used to assess the effects of clinical and pathologic characteristics, 2D MSSA, 3D MSSMPR, and 3D SV as potential prognostic factors. The significant variables at the univariable analysis were adopted for the multivariable analysis, and stepwise method was used for further variable selection. Finally, univariable and multivariable logistic regression analyses were performed to compare the association between the presence of intratumoral desmoplastic reaction and the volume partitioned by the threshold CT number of −300 HU and 0 HU.

Analyses were performed by using SPSS (version 23; IBM, Armonk, NY), Microsoft Excel 2013 (Redmond, Wash), and add-in statistical software (BellCurve, version 2.13; Social Survey Research Information, Tokyo, Japan). A P value $< .05$ was considered to indicate statistical significance.

Results

Interreader Reliability

For all size and volume measurements, the agreement of the two readers showed almost perfect agreement ($P <$ .001) (Table 2).

Table 2

Interreader Reliability for Measurement

Parameter	Interreader ICCs	*P* Value
2D MTSA	0.937 (0.907, 0.958)	<.001
2D MSSA	0.943 (0.915, 0.961)	<.001
3D MTSMPR	0.912 (0.848, 0.946)	<.001
3D MSSMPR	0.971 (0.957, 0.980)	<.001
3D total volume	0.940 (0.911, 0.959)	<.001
3D SV greater than −300 HU	0.994 (0.991, 0.996)	<.001
3D SV greater than −200 HU	0.995 (0.993, 0.997)	<.001
3D SV greater than −100 HU	0.996 (0.994, 0.997)	<.001
3D SV greater than 0 HU	0.996 (0.994, 0.997)	<.001

Note.—Data in parentheses are 95% confidence intervals. ICC = intraclass correlation coefficient, MSSA = maximal solid size on axial image, MSSMPR = maximal solid size on multiplanar reconstructed images, MTSA = maximal total size on axial image, MTSMPR = maximal total size on multiplanar reconstructed images, SV = solid volume, 3D = three-dimensional, 2D = two-dimensional.

Comparison between Recurrent and Nonrecurrent Tumors

The recurrent tumors showed significantly higher 2D MSSA, 3D MSSMPR, and 3D SV than did the nonrecurrent tumors ($P < .001$, $P < .001$, and $P = .023$ to .026, respectively) (Table 3). For pathologic invasiveness, the frequency of lymphatic and/or vascular invasion and lymph node metastasis in recurrent tumors were significantly higher than in nonrecurrent tumors ($P < .001$ and $P < .001$), whereas the frequency of pleural invasion did not differ significantly between recurrent and nonrecurrent tumors ($P = .425$).

Receiver Operating Characteristics Analysis for Predicting Postoperative Recurrence of the Tumor

The results of receiver operating characteristics analysis for predicting postoperative recurrence are shown in Table 4. For size measurements, the AUC of 2D MSSA was significantly higher than that of 2D MTSA ($P = .044$). The AUC of 3D MSSMPR was higher than that of 3D MTSMPR, but the difference was not significant ($P = .249$). In addition, no significant difference was found between 2D MSSA and 3D MSSMPR ($P = .316$). For volume measurements, the AUCs of 3D SVs were significantly higher than those of 3D TVs ($P = .003$ to .016). Particularly, 3D SV_{0HU} that defines volume of greater than 0 HU in the tumor as SV showed the highest AUC. The AUC of 3D SV_{0HU} was 0.835, and it was significantly higher than that of 3D TV, 3D SV greater than −300 HU, and 3D SV greater than −200 HU ($P = .003$, $P = .006$, and $P = .017$, respectively). The AUC of 3D SV_{0HU} was also higher than that of 3D SV greater than −100 HU, although no significant differences were found ($P = .067$). The AUC of 3D SV_{0HU} was significantly higher than that of 3D MSSMPR ($P = .017$). The AUC of 3D SV_{0HU} was also higher than that of 2D MSSA, although no significant differences were found ($P = .112$).

An appropriate 3D SV_{0HU} cutoff level for tumor recurrence determination was estimated to be 0.54 cm^3 with Youden index. This value yielded sensitivity of 0.933 (14 of 15) and specificity of 0.716 (58 of 81) in determining tumor recurrence. Figure 4 shows the Kaplan-Meier curves for disease-free survival by using this cutoff level of 3D SV_{0HU}. Patients with 3D SV_{0HU} greater than or equal to 0.54 cm^3 had a significantly worse prognosis than did those with 3D SV_{0HU} less than 0.54 cm^3 with the log-rank test ($P < .001$).

Factors Correlated with Postoperative Prognosis

At univariable analysis with Cox proportional hazards model for disease-free survival, lymphatic and/or vascular invasion, lymph node metastasis, 2D MSSA greater than 1 cm, 2D MSSA greater than 2 cm, 3D MSSMPR greater than 1 cm, 3D MSSMPR greater than 2 cm, and 3D SV_{0HU} greater than or equal to 0.54 cm^3 were significant factors correlated with postoperative prognosis ($P = .002$, $P < .001$, $P = .034$, $P = .002$, $P = .042$, $P = .017$, and $P < .001$, respectively) (Table 5). At the multivariable analysis using these seven significant factors, postoperative prognosis was significantly correlated with lymphatic and/or vascular invasion ($P = .040$) and 3D SV_{0HU} greater than or equal to 0.54 cm^3 ($P = .001$) (Table 5).

Correlation between Presence of Desmoplastic Reaction and Volume Partitioned by the CT Number

In the univariable analysis, the desmoplastic reaction was significantly correlated with the volume of −299 HU to 0 HU and the volume of greater than 0 HU ($P = .016$ and $P = .007$, respectively) (Table 6). Furthermore, the multivariable analysis demonstrated that only the volume of greater than 0 HU was a significant factor ($P = .004$) (Table 6). The CT and pathologic findings of the recurrent and nonrecurrent part-solid tumors are shown in Figures 5 and 6.

Discussion

Our study shows that computer-aided volumetry of solid component in subsolid lung cancers at multidetector CT more accurately correlated with postoperative recurrence than did 2D and 3D diametrical measurements of the solid component. The receiver operating characteristics analysis illustrated that 2D MSSA and 3D MSSMPR showed higher diagnostic accuracy of postoperative recurrence than did 2D MTSA and 3D MTSMPR, respectively. Our results are consistent with previous studies showing that the tumor solid size or its proportion to the total size in lung adenocarcinomas is associated with tumor invasiveness and postoperative prognosis (5,18,19). Similarly, 3D SV showed higher diagnostic accuracy for recurrence than did 3D TV in our study. Furthermore, the diagnostic accuracy of 3D SV was higher than those

Table 3

Recurrence versus Nonrecurrence

Parameter	Recurrence ($n = 15$)	Nonrecurrence ($n = 81$)	*P* Value
No. of women	7	42	…
Age (y)	70 ± 7	65 ± 8	.175
No. of men	8	39	…
Age (y)	66 ± 9	65 ± 6	.811
Postoperative follow-up duration (mo)	26 ± 14	67 ± 26	<.001
Range (mo)	1–41	8–120	…
Pleural invasion*	7 (47)	29 (36)	.425
Lymphatic and/or vascular invasion*	5 (33)	4 (5)	<.001
Lymph node metastasis*	5 (33)	2 (2)	<.001
Desmoplastic reaction*	9 (60)	30 (37)	.056
2D MTSA (cm)	2.88 ± 0.74	2.30 ± 0.87	.018
2D MSSA (cm)	2.03 ± 0.57	1.24 ± 0.76	< .001
3D MTSMPR (cm)	3.46 ± 1.05	2.65 ± 1.10	.010
3D MSSMPR (cm)	2.46 ± 1.02	1.47 ± 0.94	< .001
3D total volume (cm^3)	7.94 ± 5.99	4.44 ± 3.72	.044
3D SV greater than −300 HU (cm^3)	4.33 ± 3.78	1.81 ± 2.27	.024
3D SV greater than −200 HU (cm^3)	3.78 ± 3.45	1.47 ± 2.04	.023
3D SV greater than −100 HU (cm^3)	3.16 ± 3.06	1.14 ± 1.74	.024
3D SV greater than 0 HU (cm^3)	2.12 ± 2.16	0.72 ± 1.18	.026

Note.—Unless otherwise specified, data are means ± standard deviation. MSSA = maximal solid size on axial image, MSSMPR = maximal solid size on multiplanar reconstructed images, MTSA = maximal total size on axial image, MTSMPR = maximal total size on multiplanar reconstructed images, SV = solid volume, 3D = three-dimensional, 2D = two-dimensional.

* Data are the number of patients, with percentages in parentheses.

Table 4

Receiver Operating Characteristics Analysis for Prediction of Tumor Recurrence

Parameter	Area Under the Curve*	Cutoff Value	Sensitivity†	Specificity†
2D MTSA (cm)	0.721 (0.588, 0.853)	2.45	0.800 (12/15)	0.617 (50/81)
2D MSSA (cm)	0.796 (0.692, 0.900)	1.70	0.800 (12/15)	0.704 (57/81)
3D MTSMPR (cm)	0.733 (0.609, 0.858)	2.65	0.867 (13/15)	0.543 (44/81)
3D MSSMPR (cm)	0.776 (0.667, 0.886)	1.75	0.800 (12/15)	0.679 (55/81)
3D total volume (cm^3)	0.695 (0.547, 0.842)	4.09	0.733 (11/15)	0.630 (51/81)
3D SV greater than −300 HU (cm^3)	0.779 (0.665, 0.892)	1.56	0.867 (13/15)	0.679 (55/81)
3D SV greater than −200 HU (cm^3)	0.802 (0.698, 0.906)	1.33	0.867 (13/15)	0.704 (57/81)
3D SV greater than −100 HU (cm^3)	0.820 (0.725, 0.915)	1.03	0.867 (13/15)	0.741 (60/81)
3D SV greater than 0 HU (cm^3)	0.835 (0.749, 0.922)	0.54	0.933 (14/15)	0.716 (58/81)

Note.—MSSA = maximal solid size on axial image, MSSMPR = maximal solid size on multiplanar reconstructed images, MTSA = maximal total size on axial image, MTSMPR = maximal total size on multiplanar reconstructed images, SV = solid volume, 3D = three-dimensional, 2D = two-dimensional.

* Data in parentheses are 95% confidence intervals.

† Data in parentheses are numerators and denominators.

of 2D MSSA and 3D MSSMPR. Conventional 2D diametrical measurement is the simplest procedure to evaluate the size of the solid component. However, the solid component in subsolid tumors often shows both spherical and irregular shapes. For an irregular solid component, the one-dimensional measurement of the diameter does not accurately represent the volume. Even if the maximal diameter was measured on the multiplanar reconstructed images, the diagnostic accuracy to predict recurrence would not improve. Therefore, 3D measurement of the SV is essential to improve the diagnostic accuracy of recurrence. Traditionally, the volumetry on 3D CT images requires manual registration of the region of interest on many thin-section images, and is therefore time consuming. More recently, computer-aided volumetry software has become commercially available; it is now feasible to routinely calculate both the TV and the SV of the tumor with greater reproducibility than the manual measurement of tumor diameter.

To decide on the optimal border of the CT number between the ground-glass and solid component, we changed the threshold value of 3D SV from −300 HU to 0 HU and performed receiver operating characteristics analysis for postoperative recurrence. We found that using a cutoff value of 0 HU had the highest AUC. By using this cutoff value, the appropriate cutoff volume of solid component was 0.54 cm^3 with high sensitivity of 0.933 and specificity of 0.716 for the differentiation between recurrent and nonrecurrent tumors. The value of 0.54 cm^3 is close to 0.52 cm^3, which is the volume of a sphere with 1 cm in diameter, and comparable to the border between T1a and T1b in TNM classification (2,10). The Kaplan-Meier curves for disease-free survival showed significantly better survival in patients with 3D SV_{0HU} less than 0.54 cm^3 than in patients with 3D SV_{0HU} greater than or equal to 0.54 cm^3. Use of 0 HU as the cutoff density value between the ground-glass and solid component is somewhat higher than what has been previously reported. Okada et al reported that the maximal CT number of ground-glass opacity by visual assessment was −194 HU (20). Matsuguma et al and Yoshida et al adopted −160 HU as the boundary value based on the visual assessment of the solid area on the lung window settings

(7,21). Shikuma et al adopted −300 HU as the boundary value, although the reason was not specified (14). The visually assessed solid component included both intratumoral collapse and fibrosis and intratumoral fibrosis associated with tumor invasiveness and prognosis (16,22). Therefore, we speculated that the higher opacity volume in the solid component may reflect the amount of fibrosis, or packed viable cells, that is associated with poor prognosis in adenocarcinomas. We further examined the relationship between intratumoral fibrosis and 3D SV by using a threshold value of 0 HU. As a consequence, the multivariable logistic regression analysis indicated that 3D SV_{0HU} was more strongly correlated with the presence of intratumoral fibrosis than with the volume from −299 HU to 0 HU. In addition, densely packed viable cells might contribute to the higher opacity volume.

Finally, we investigated whether the clinical, pathologic, and radiologic findings were significantly correlated with disease-free survival by using the Cox proportional hazards model. Multivariable analysis revealed that 3D SV_{0HU} in the radiologic findings was an independent prognostic factor. The conventional 2D MSSA and 3D MSSMPR were also significant at the univariable analysis, although they did not remain significant at the multivariable analysis. This indicates that 3D SV_{0HU} allows for a more accurate prediction of the postoperative prognosis prior to surgery than can be accomplished by using 2D MSSA and 3D MSSMPR. Among the pathologic invasive findings, intratumoral vessel invasion (lymphatic and/or vascular invasion) was significant but pleural invasion was not. The reason that pleural invasion did not show an association with disease-free survival may have been because it is related to both tumor invasiveness and distance from the tumor to the pleura.

Figure 4

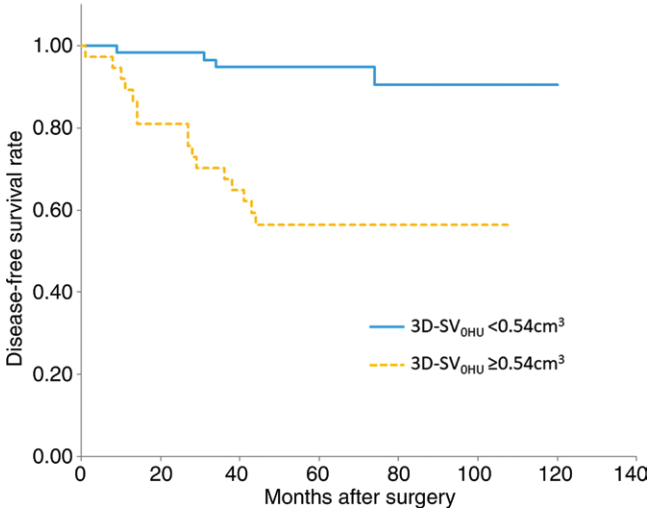

Figure 4: Graph shows Kaplan-Meier curves for disease-free survival based on cutoff level of three-dimensional (3D) solid volume of greater than 0 HU (hereafter, 3D SV_{0HU}) of 0.54 cm^3. Patients with 3D SV_{0HU} greater than or equal to 0.54 cm^3 had a significantly worse prognosis than did those with 3D SV_{0HU} less than 0.54 cm^3 with log-rank test ($P < .001$).

Table 5

Univariable and Multivariable Analyses with Cox Proportional Hazards Model for Disease-free Survival

	Univariable		Multivariable	
Factor	Hazard Ratio	*P* Value	Hazard Ratio	*P* Value
Age (y)	1.016 (0.958, 1.078)	.590	…	…
Female vs male	0.976 (0.406, 2.346)	.957	…	…
Limited surgery vs standard surgery	0.741 (0.217, 2.529)	.632	…	…
Pleural invasion	1.626 (0.676, 3.910)	.277	…	…
Lymphatic and/or vascular invasion	4.822 (1.744, 13.336)	.002	2.955 (1.050, 8.318)	.040
Lymph node metastasis	6.203 (2.242, 17.161)	<.001	…	…
2D MSSA >1 cm	3.773 (1.106, 12.877)	.034	…	…
2D MSSA >2 cm	4.110 (1.708, 9.889)	.002	…	…
3D MSSMPR >1 cm	4.565 (1.059, 19.681)	.042	…	…
3D MSSMPR >2 cm	2.937 (1.216, 7.091)	.017	…	…
3D solid volume greater than 0 HU ≥0.54 cm^3	7.622 (2.546, 22.819)	<.001	6.607 (2.168, 20.135)	.001

Note.—Data in parentheses are 95% confidence intervals. MSSA = maximal solid size on axial image, MSSMPR = maximal solid size on multiplanar reconstructed images, MTSA = maximal total size on axial image, MTSMPR = maximal total size on multiplanar reconstructed images, 3D = three-dimensional, 2D = two-dimensional.

The reason that lymph node metastasis did not show an association with disease-free survival at the multivariable analysis may have been because of both the small number of lymph node metastases in this cohort and confounding issues related to lymphatic and/or vascular invasion.

For non–small cell lung cancer resected surgically, many pathologic and genetic factors have been reported to define prognosis (23–25). The pathologic invasive size of the surgical specimen that is correlated with the solid size at thin-section CT is a representative prognostic factor (2,26,27). Recently, stereotactic radiation therapy has been gaining attention as an alternative therapy; however, the pathologic prognostic factors are limited for this therapy. The standardized uptake value of primary lung cancer at fluorine 18 fluorodeoxyglucose positron emission

Table 6

Univariable and Multivariable Logistic Regression Analyses for the Presence of Desmoplastic Reaction within the Tumor

	Univariable		Multivariable	
Factor	Odds Ratio	*P* Value	Odds Ratio	*P* Value
Volume of less than or equal to −300 HU (cm^3)	0.696 (0.463, 1.048)	.083	0.803 (0.635, 1.016)	.067
Volume of −299 HU to 0 HU (cm^3)	1.537 (1.084, 2.179)	.016	…	…
Volume greater than 0 HU (cm^3)	1.786 (1.177, 2.710)	.007	2.291 (1.311, 4.007)	.004

Note.—Data in parentheses are 95% confidence intervals.

Figure 5

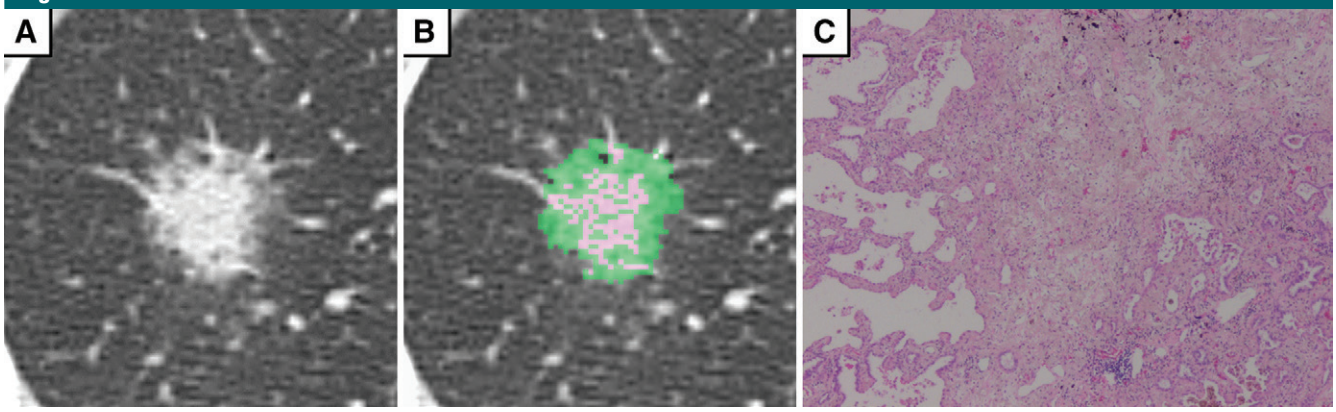

Figure 5: Images show CT and pathologic findings of nonrecurrent part-solid nodule. *A,* Axial CT image. *B,* Three-dimensional (3D) solid volume (hereafter, 3D SV) image. Pink area on nodule shows solid part greater than 0 HU and measured value of 3D SV of greater than 0 HU is 0.78 cm^3. *C,* Histopathologic image stained with hematoxylin and eosin (original magnification, ×40). Central solid part of tumor mostly consists of collapse and no fibrosis is seen.

Figure 6

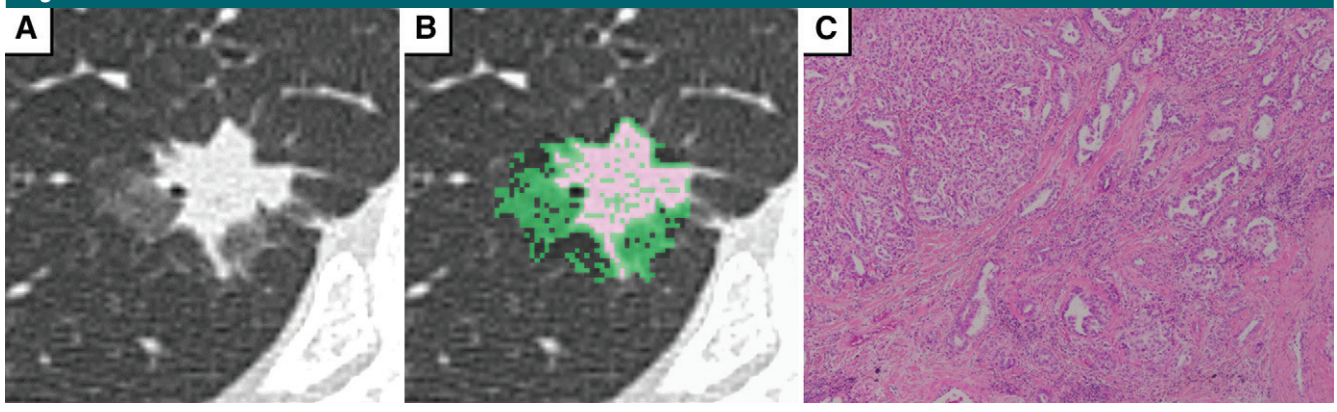

Figure 6: Images show CT and pathologic findings of recurrent part-solid nodule. *A,* Axial CT image. *B,* Three-dimensional (3D) solid volume (hereafter, 3D SV) image. Pink area on nodule shows solid part greater than 0 HU and measured value of 3D SV of greater than 0 HU is 1.16 cm^3. *C,* Histopathologic image stained with hematoxylin and eosin (original magnification, × 40). Central part of tumor mostly consists of densely packed viable tumor cells and fibrosis.

tomographic/CT imaging is well known as an effective predictor. Yet for subsolid tumors, the solid size or solid size ratio to the total size at thin-section CT are more informative (19). For subsolid tumors, the 3D SV may be an alternative biomarker to conventional solid size measurements as a predictor of prognosis.

Our study had some limitations. First, it was a retrospective and single-center study. Therefore, multicenter study may be necessary in the future. Second, the number of recurrent tumors in this cohort was relatively small because subsolid non–small cell lung cancers typically have a good prognosis (19,28). Moreover, the recent development of a tyrosine kinase inhibitor effective against most adenocarcinomas with specific genetic mutations has improved the life prognosis of patients with recurrence (29). Therefore, overall survival as an outcome could not be analyzed. Third, total size and solid size were measured manually without using computer-aided diagnosis. If computer-aided diagnosis could calculate the maximal diameter of the solid component in the tumor segmented at the same time as volumetry, then interreader accordance of 2D MSSA and 3D MSSMPR would improve. Fourth, we selected at random only 50 patients from the 150 patients with nonrecurrent and noninvasion as a control group in this case-control study. Because all of the 150 patients at our institution were not included in the cohort, this might result in slight statistical error. However, the selection made appropriately by using a random number table hardly affect the results. Fifth, pathologic invasive size was not measured in this study because our cohort included old cases and the pathologists at the time did not measure it. However, previous studies reported that the pathologic invasive size was correlated with solid size (2,26,27).

In conclusion, the volumetry of the solid component of part-solid non–small cell lung cancer shows better correlation with postoperative recurrence and prognosis than does the conventional diameter measurement. We found that the SV_{0HU} was most strongly correlated with recurrence; tumor volume of greater than or equal to 0.54 cm^3 indicated poor prognosis.

Disclosures of Conflicts of Interest: S.K. disclosed no relevant relationships. **S.I.** disclosed no relevant relationships. **H.U.** disclosed no relevant relationships. **R.I.** disclosed no relevant relationships. **H.S.** disclosed no relevant relationships. **Shota Nakamura** disclosed no relevant relationships. **Shinji Naganawa** disclosed no relevant relationships.

References

1. Yeh YC, Kadota K, Nitadori J, et al. International Association for the Study of Lung Cancer/American Thoracic Society/European Respiratory Society classification predicts occult lymph node metastasis in clinically mediastinal node-negative lung adenocarcinoma. Eur J Cardiothorac Surg 2016;49(1):e9–e15.
2. Travis WD, Asamura H, Bankier AA, et al. The IASLC lung cancer staging project: proposals for coding T categories for subsolid nodules and assessment of tumor size in part-solid tumors in the forthcoming eighth edition of the TNM classification of lung cancer. J Thorac Oncol 2016;11(8):1204–1223.
3. Travis WD, Brambilla E, Nicholson AG, et al. The 2015 World Health Organization classification of lung tumors: impact of genetic, clinical and radiologic advances since the 2004 classification. J Thorac Oncol 2015;10(9):1243–1260.
4. Van Schil PE, Sihoe AD, Travis WD. Pathologic classification of adenocarcinoma of lung. J Surg Oncol 2013;108(5):320–326.
5. Nakamura S, Fukui T, Taniguchi T, et al. Prognostic impact of tumor size eliminating the ground glass opacity component: modified clinical T descriptors of the tumor, node, metastasis classification of lung cancer. J Thorac Oncol 2013;8(12):1551–1557.
6. Saji H, Matsubayashi J, Akata S, et al. Correlation between whole tumor size and solid component size on high-resolution computed tomography in the prediction of the degree of pathologic malignancy and the prognostic outcome in primary lung adenocarcinoma. Acta Radiol 2015;56(10):1187–1195.
7. Yoshida Y, Sakamoto M, Maeda E, et al. Can image analysis on high-resolution computed tomography predict non-invasive growth in adenocarcinoma of the lung? Ann Thorac Cardiovasc Surg 2015;21(1):8–13.
8. Liu Y, Sun H, Zhou F, et al. Imaging features of TSCT predict the classification of pulmonary preinvasive lesion, minimally and invasive adenocarcinoma presented as ground glass nodules. Lung Cancer 2017;108:192–197.
9. Ahn SY, Park CM, Jeon YK, et al. Predictive CT features of visceral pleural invasion by T1-sized peripheral pulmonary adenocarcinomas manifesting as subsolid nodules. AJR Am J Roentgenol 2017;209(3):561–566.
10. Aokage K, Miyoshi T, Ishii G, et al. Clinical and pathological staging validation in the eighth edition of the TNM classification for lung cancer: correlation between solid size on thin-section computed tomography and invasive size in pathological findings in the new T classification. J Thorac Oncol 2017;12(9):1403–1412.
11. Iwano S, Okada T, Koike W, et al. Semi-automatic volumetric measurement of lung cancer using multi-detector CT effects of nodule characteristics. Acad Radiol 2009;16(10):1179–1186.
12. Takenaka T, Yamazaki K, Miura N, Mori R, Takeo S. The prognostic impact of tumor volume in patients with clinical stage IA non-small cell lung cancer. J Thorac Oncol 2016;11(7):1074–1080.
13. Ohno Y, Yaguchi A, Okazaki T, et al. Comparative evaluation of newly developed model-based and commercially available hybrid-type iterative reconstruction methods and filter back projection method in terms of accuracy of computer-aided volumetry (CADv) for low-dose CT protocols in phantom study. Eur J Radiol 2016;85(8):1375–1382.
14. Shikuma K, Menju T, Chen F, et al. Is volumetric 3-dimensional computed tomography useful to predict histological tumour invasiveness? Analysis of 211 lesions of cT-1N0M0 lung adenocarcinoma. Interact Cardiovasc Thorac Surg 2016;22(6):831–838.
15. Liang M, Yip R, Tang W, et al. Variation in screening CT-detected nodule volumetry as a function of size. AJR Am J Roentgenol 2017;209(2):304–308.
16. Maeshima AM, Niki T, Maeshima A, Yamada T, Kondo H, Matsuno Y. Modified scar grade: a prognostic indicator in small peripheral lung adenocarcinoma. Cancer 2002;95(12):2546–2554.
17. Landis JR, Koch GG. The measurement of observer agreement for categorical data. Biometrics 1977;33(1):159–174.
18. Uehara H, Tsutani Y, Okumura S, et al. Prognostic role of positron emission tomography and high-resolution computed tomography in clinical stage IA lung adenocarcinoma. Ann Thorac Surg 2013;96(6):1958–1965.
19. Kishimoto M, Iwano S, Ito S, Kato K, Ito R, Naganawa S. Prognostic evaluations of small size lung cancers by 18F-FDG PET/CT and thin-section CT. Lung Cancer 2014;86(2):180–184.

20. Okada T, Iwano S, Ishigaki T, et al. Computer-aided diagnosis of lung cancer: definition and detection of ground-glass opacity type of nodules by high-resolution computed tomography. Jpn J Radiol 2009;27(2):91–99.

21. Matsuguma H, Nakahara R, Anraku M, et al. Objective definition and measurement method of ground-glass opacity for planning limited resection in patients with clinical stage IA adenocarcinoma of the lung. Eur J Cardiothorac Surg 2004;25(6):1102–1106.

22. Noguchi M, Morikawa A, Kawasaki M, et al. Small adenocarcinoma of the lung: histologic characteristics and prognosis. Cancer 1995;75(12):2844–2852.

23. Shoji F, Haro A, Yoshida T, et al. Prognostic significance of intratumoral blood vessel invasion in pathologic stage IA non-small cell lung cancer. Ann Thorac Surg 2010;89(3):864–869.

24. Chen T, Luo J, Wang R, et al. Visceral pleural invasion predict a poor survival among lung adenocarcinoma patients with tumor size ≤ 3cm. Oncotarget 2017;8(39):66576–66583.

25. Fan G, Zhang K, Ding J, Li J. Prognostic value of EGFR and KRAS in circulating tumor DNA in patients with advanced non-small cell lung cancer: a systematic review and meta-analysis. Oncotarget 2017;8(20):33922–33932.

26. Tsutani Y, Miyata Y, Nakayama H, et al. Solid tumor size on high-resolution computed tomography and maximum standardized uptake on positron emission tomography for new clinical T descriptors with T1 lung adenocarcinoma. Ann Oncol 2013;24(9):2376–2381.

27. Sakakura N, Inaba Y, Yatabe Y, et al. Estimation of the pathological invasive size of pulmonary adenocarcinoma using high-resolution computed tomography of the chest: a consideration based on lung and mediastinal window settings. Lung Cancer 2016;95:51–56.

28. Hattori A, Matsunaga T, Takamochi K, Oh S, Suzuki K. Importance of ground glass opacity component in clinical stage IA radiologic invasive lung cancer. Ann Thorac Surg 2017;104(1):313–320.

29. Huang Q, Li J, Sun Y, Wang R, Cheng X, Chen H. Efficacy of EGFR tyrosine kinase inhibitors in the adjuvant treatment for operable non-small cell lung cancer by a meta-analysis. Chest 2016;149(6):1384–1392.